Advances in Clinical Radiology 1 (2019) 27–41
ADVANCES IN CLINICAL RADIOLOGY

Cardiac MRI T1, T2, and T2* Mapping in Clinical Practice

Gauri Rani Karur, MD, Kate Hanneman, MD, MPH, FRCPC*
Department of Medical Imaging, Toronto General Hospital, 585 University Avenue, 1PMB-298, Toronto, Ontario M5G 2N2, Canada

KEYWORDS
• Cardiac MRI • T1 mapping • T2 mapping • T2* mapping • Extracellular volume fraction

KEY POINTS

- Cardiac MRI T1, T2, and T2* parametric mapping techniques allow both visual and quantitative myocardial assessment, detecting focal and global tissue changes.
- Native T1 and extracellular volume values are increased in the setting of myocardial fibrosis, edema, and amyloid. Native T1 values are decreased in the setting of myocardial iron, hemorrhage, and Fabry disease.
- Native T2 values are increased in the setting of edema, including acute myocardial infarction, myocarditis, and stress-induced cardiomyopathy. Native T2 values are decreased in the setting of myocardial iron.
- T2* values are decreased in the setting of iron and hemorrhage.

INTRODUCTION

Cardiac MRI is considered the gold standard for quantification of myocardial volumes, function, and mass [1]. A key strength of cardiac MRI compared with other imaging modalities is its ability to characterize tissue. Cardiac MRI tissue characterization previously relied on qualitative techniques such as late gadolinium enhancement (LGE) imaging and T2-weighted imaging. However, these conventional techniques are limited by observer subjectivity and difficulty characterizing diffuse myocardial changes, such as interstitial fibrosis. With recent technological advancements, parametric mapping of magnetic relaxation properties (T1, T2, and T2*) has become feasible and is increasingly being integrated into routine clinical practice. Parametric mapping allows for both visual and quantitative myocardial assessment, including focal and diffuse tissue changes such as fibrosis, edema, amyloid deposition, and iron overload. Another advantage of quantitative parametric tissue characterization is the potential to monitor changes over time in relation to disease progression and treatment response. Absolute parametric values differ depending on many factors, including field strength and the specific sequence used, and therefore should be evaluated against local reference ranges [2,3]. This article reviews T1, T2, and T2* mapping techniques and clinical applications.

SIGNIFICANCE

Technical Considerations

Cardiac MRI parametric mapping techniques allow visualization and quantification of myocardial tissue changes based on T1, T2, and T2* relaxation times. T1, T2, and T2* are intrinsic magnetic properties of all tissues. Each pixel in a parametric map represents a specific magnetic tissue property that is derived from the

Disclosures: None.

*Corresponding author, *E-mail address:* kate.hanneman@uhn.ca

https://doi.org/10.1016/j.yacr.2019.03.001
2589-8744/19/

corresponding voxel of a set of coregistered source images.

T1 mapping

The T1 relaxation time, also referred to as spin-lattice or longitudinal relaxation, is determined by how rapidly protons reequilibrate their spins after excitation by a radiofrequency pulse. Most acquisition schemes used to sample the T1 recovery signal use multiple single-shot balanced steady state free precession (SSFP) acquisitions, classified as inversion preparation, saturation preparation, or combination techniques [4]. Inversion recovery techniques include modified Look-Locker inversion recovery (MOLLI), shortened MOLLI (shMOLLI), and variants. These sequences have potential bias from T2 and are prone to magnetization transfer effects caused by the SSFP readout [4]. Although inversion recovery techniques have the advantage of high precision, they are limited by heart rate dependence and lower accuracy compared with saturation recovery techniques, such as saturation recovery single-shot acquisition (SASHA) [2].

T1 maps can be acquired without administering gadolinium-based contrast (native T1 maps) or following administration of intravenous contrast (postcontrast T1 maps). Postcontrast T1 maps have higher variability compared with native T1 maps because of contrast-related factors such as the volume and concentration of contrast administered, and therefore should not be interpreted in isolation in clinical practice [5]. However, postcontrast T1 maps can be used in combination with native T1 values to calculate the extracellular volume (ECV) fraction according to the following formula [6]:

$$ECV = (1 - \text{hematocrit}) \times (1/T1_{\text{myocardium postcontrast}} - 1/T1_{\text{myocardium native}})/(1/T1_{\text{blood pool postcontrast}} - 1/T1_{\text{blood pool native}}).$$

ECV is an estimate of the proportion of extracellular space within the myocardium. Calculation of ECV requires input of hematocrit, which is typically acquired by venipuncture. Alternative sampling methods for hematocrit include use of noninvasive point-of-care devices and calculation of synthetic hematocrit based on the relationship between hematocrit and blood pool native T1 time [7,8]. Accurate assessment of hematocrit is important because ECV can vary significantly depending on the timing of hematocrit evaluation [9].

Native T1 times vary according to technical factors (such as magnetic field strength, cardiac phase, the myocardial region evaluated, and the specific sequence used) and patient-related factors (such as heart rate, age, and sex) [10–12]. Importantly, native T1 values are approximately 25% higher when acquired at 3 T compared with 1.5 T [12,13]. Native T1 values are approximately 15% lower when acquired using inversion recovery–based acquisition schemes compared with saturation recovery schemes [2,14]. Native T1 and T2 values have been shown to increase from base to apex, possibly because of partial-volume effects that increase toward the apex related to left ventricular geometry [15]. Native T1 values at the interventricular septum are higher compared with lateral segments [16]. Although patient-related factors can influence T1 values, age-related and sex-related differences in native T1 values are estimated at only approximately 0.5 standard deviations from the normal mean [16,17].

ECV is derived from the ratio of precontrast and postcontrast T1 values and therefore may be less variable compared with absolute T1 values [18]. ECV is not significantly associated with the myocardial region sampled, age, or sex [5,16]. However, ECV values have been shown to vary depending on the sequence used [19,20]. ECV values by inversion recovery techniques have been reported to be higher compared with saturation recovery methods [2]. Published normal reference ranges for native T1 and ECV values are provided in Table 1.

T2 mapping

The T2 relaxation time, also referred to as spin-spin or transverse relaxation, can be determined from T2 maps, generated by obtaining a series of images to calculate a T2 decay curve. Multiple different T2 mapping techniques have been described. In general, a T2 preparation pulse is applied to impart T2 signal contrast with a subsequent readout [21]. According to current guidelines, T2-prepared balanced SSFP or gradient echo pulse sequences with a minimum of 3 source images are recommended [17]. T2 maps are acquired without administration of contrast (native T2).

Similar to T1 values, native T2 times vary according to multiple factors, including field strength and the specific sequence used. SSFP-based T2-mapping techniques result in slightly higher T2 values compared with fast low-angle shot (FLASH) sequences but offer more signal to noise and less image artifact [21–23]. Absolute T2 values are approximately 10% lower when acquired at 3 T compared with 1.5 T [15,23,24]. Female sex and increasing age may be associated with increased myocardial T2 values acquired at 1.5 T [25]. However, other studies report that age and sex are not associated

TABLE 1
Normal reference ranges for myocardial native T1 and extracellular volume values

Reference	Scanner	Technique	Sample Size (n)	Population	Native T1 (ms)	ECV (%)
1.5 T						
Messroghli et al [10], 2006	1.5 T (Gyroscan Intera CV, Philips, Best, The Netherlands)	MOLLI, 8-mm slice thickness, 3 short-axis slices	15	Age range 21–49 y (33.1 ± 8.5 y), 60% men	980 ± 53	—
Kellman et al [108], 2012	1.5 T (Avanto and Espree, Siemens Healthcare, Erlangen, Germany)	MOLLI, 6-mm slice thickness, short-axis and 4-chamber slices	62	Mean age 44 ± 17 y, 48% men	965 ± 35, range 894–1035	25.4 ± 2.5, range 20.4–30.4
Liu et al [109], 2013	1.5 T (Avanto and Espree, Siemens Healthcare, Erlangen, Germany)	MOLLI, 8-mm slice thickness, midventricular short-axis slice	1231	Age range 54–93 y, 49% men	986 ± 45 (women); 968 ± 38 (men)	28.1 ± 2.8 (women); 25.8 ± 2.1 (men)
Piechnik et al [110], 2013	1.5 T (Avanto, Siemens Healthcare, Erlangen, Germany)	ShMOLLI, 8-mm slice thickness, short-axis slices	342	Age range 11–69 y, 50% men	962 ± 25	—
Chow et al [111], 2014	1.5 T (Avanto, Siemens Healthcare, Erlangen, Germany)	SASHA, 8-mm slice thickness, midventricular short-axis slice	19	Mean age 28 ± 6 y, 58% men	1174 ± 27	—
Reiter et al,[112] 2014	1.5 T (Espree, Siemens Healthcare, Erlangen, Germany)	MOLLI, 8-mm slice thickness, 3 short-axis slices in systole and diastole	40	Age range 20–35 y, 50% men	984 ± 28 (diastole); 959 ± 21 (systole)	—
Dabir et al [113], 2014	1.5 T (Achieva or Ingenia, Philips Healthcare, Best, The Netherlands)	MOLLI, 8-mm slice thickness, midventricular short-axis slice	102	Age range 17–83 y (41 ± 17 y), 52% men	950 ± 21	25 ± 4
Rauhalammi et al [16], 2016	1.5 T (Avanto, Siemens Healthcare, Erlangen, Germany)	MOLLI, 8-mm slice thickness, 3 short-axis slices	84	Mean age 45 ± 18, 49% men	944 ± 25 (global); 956 ± 44 (septum); 939 ± 54 (lateral)	—

(*continued on next page*)

TABLE 1
(*continued*)

Reference	Scanner	Technique	Sample Size (n)	Population	Native T1 (ms)	ECV (%)
3 T						
Von Knobelsdorff-Brenkenhoff et al [15], 2013	3.0 T (Verio, Siemens Healthcare, Erlangen, Germany)	MOLLI, 6-mm slice thickness, 3 short-axis slices	60	Mean age 48 ± 17 y, 50% men	Mean values: 1157 (base), 1159 (mid), 1181 (apex)	—
Dabir et al [113], 2014	3.0 T (Achieva or Ingenia, Philips Healthcare, Best, The Netherlands)	MOLLI, 8-mm slice thickness, midventricular short-axis slice	102	Age range 17–83 y, 52% men	1052 ± 23	26 ± 4
Rauhalammi et al [16], 2016	3.0 T (Verio, Siemens Healthcare, Erlangen, Germany)	MOLLI, 8-mm slice thickness, 3 short-axis slices	84	Mean age 45 ± 18, 49% men	1155 ± 26 (global); 1158 ± 46 septum); 1149 ± 57 (lateral	—
Teixeira et al [14], 2016	3.0 T (Skyra, Siemens Healthcare, Erlangen, Germany)	MOLLI, ShMOLLI, and SASHA, 8-mm slice thickness, short-axis slice	9	Mean age 58 ± 11, 33% men	1208 ± 18 (MOLLI); 1178 ± 29 (ShMOLLI); 1486 ± 24 (SASHA)	—
Roy et al [11], 2017	3.0 T (Ingenia, Philips Healthcare, Best, The Netherlands)	MOLLI, 6-mm slice thickness, short-axis and 4-chamber slices	75	Age range 20–90 y (56 ± 19 y), 53% men	1122 ± 57, range 977–1225 (global); 1162 ± 81, range 954–1285 (septum)	26.6 ± 3.2, range 21.6–34.5 (global); 27.5 ± 3.8, range 21.0–37.6 (septum)

with T2 values when acquired at 3 T [15]. Published normal reference ranges for native T2 values are provided in Table 2.

T2 mapping*

T2* is a time constant representing the decay of transverse magnetization in the presence of local field inhomogeneities. T2* decay can be exploited in the detection of inherently inhomogeneous tissues with magnetic susceptibility effects such as iron [26]. Hemosiderin and ferritin create susceptibility-induced distortions in the magnetic field, which result in much faster decay of transverse magnetization than would be expected for true T2. T2* is always less than or equal to T2.

T2* maps can be generated by acquiring a series of images using a multiecho gradient sequence. Current clinical guidelines recommend that T2* mapping should be performed at 1.5 T with 8 equally spaced echoes ranging from 2 to 18 milliseconds [17]. At present, both bright-blood and black-blood T2* techniques are validated and used clinically [27,28]. Black-blood techniques show less bias and reduced interobserver variability, and therefore are recommended if available [29]. T2* analysis is typically limited to the septum to reduce susceptibility artifacts. T2* values

TABLE 2
Normal reference ranges for myocardial native T2 values

Reference	Scanner	Technique	Sample Size (n)	Population	Native T2 (ms)
1.5 T					
Giri et al [114], 2012	1.5 T (Avanto, Siemens Healthcare, Erlangen, Germany)	T2-prepared single-shot SSFP, 8-mm slice thickness, 3 short-axis slices	10	—	52.3 ± 6.5
Wassmuth et al [21], 2013	1.5 T (Avanto, Siemens Healthcare, Erlangen, Germany)	T2 prepared SSFP and FLASH, 8-mm slice thickness, midventricular short-axis slice	73	Age range 20–70 y (35 ± 13 y), 82% men	55 ± 5, range 46–69 (SSFP); 52 ± 5, range 41–62 (FLASH)
Baeßler et al [24], 2015	1.5 T (Achieva, Philips Healthcare, Best, The Netherlands)	MESE, T2-prepared balanced SSFP, and multiecho GRASE	30	Mean age 36 ± 13 y, 47% men	53.8 ± 2.7 (MESE); 52.5 ± 2.5 (SSFP); 58.6 ± 4.2 (GRASE)
3 T					
Von Knobelsdorff-Brenkenhoff et al [15], 2013	3.0 T (Verio, Siemens Healthcare, Erlangen, Germany)	T2-prepared single-shot SSFP, 6-mm slice thickness, 3 short-axis slices	60	Mean age 48 ± 17 y, 50% men	Mean values: 44 (base), 45 (middle), 47 (apex)
Baeßler et al [24], 2015	3.0 T (Achieva, Philips Healthcare, Best, The Netherlands)	MESE, T2-prepared balanced SSFP, and multiecho GRASE	30	Mean age 36 ± 13 y, 47% men	52.0 ± 3.6 (MESE); 44.0 ± 3.2 (SSFP); 54.2 ± 4.1 (GRASE)
Roy et al [11], 2017	3.0 T (Ingenia, Philips Healthcare, Best, The Netherlands)	Multiecho GRASE, 10-mm slice thickness, midventricular short-axis slice	75	Age range 20–90 y (56 ± 19 y), 53% men	52 ± 6, range 41–61 (global); 52 ± 7, range 38–64 (septum)

Abbreviations: GRASE, gradient spin echo; MESE, multiecho spin echo.

are not associated with age or sex; however values are lower when acquired at 3 T compared with 1.5 T [11]. Published normal reference ranges for T2* values are provided in Table 3.

Clinical Applications

Myocardial tissue has a characteristic range of T1, T2, T2*, and ECV values, which can be altered in disease. Pathologic tissue changes that can be detected using parametric mapping techniques include intracellular disturbances of cardiomyocytes (such as iron overload and Fabry disease), extracellular disturbances of the interstitium (such as fibrosis and amyloidosis), and processes that can affect both intracellular and extracellular components (such as edema) [17].

The extent and pattern of change in myocardial parametric values varies by disease process. Some diseases alter values substantially (such as amyloid and myocardial infarction), whereas other diseases have smaller effects (such as interstitial fibrosis in the setting of

TABLE 3
Normal reference ranges for myocardial T2* values

Reference	Scanner	Technique	Sample Size (n)	Population	T2* (ms)
1.5 T					
Westwood et al [115], 2003	1.5 T (Sonata, Siemens Healthcare, Erlangen, Germany)	Single-breath-hold, segmented, multiecho gradient echo sequence using 9 echoes, midventricular short-axis slice	10	Mean age 49 ± 26 y, 30% men	33.3 ± 7.8 (septum)
Pepe et al [116], 2006	1.5 T (CV/i, GE, Milwaukee, WI)	Single-breath-hold, segmented, multiecho gradient echo sequence using 9 echoes, 8-mm slice thickness, 3 short-axis slices	20	Mean age 33 ± 9 y, 70% men	36.4 ± 6.7 (midseptum); 35.2 ± 4.3 (global)
Kirk et al [117], 2010	1.5 T (Sonata, Siemens Healthcare, Erlangen, Germany)	Single-breath-hold, segmented, multiecho gradient echo sequence using 8 echoes, midventricular short-axis slice	63	Age range 18–77 y (42.3 ± 14.6 y), 60% men	Median 36.3, interquartile range 31.6–45.4 (septum)
3 T					
Roy et al [11], 2017	3.0 T (Ingenia, Philips Healthcare, Best, The Netherlands)	Single-breath-hold, segmented, multiecho gradient echo sequence using 8 echoes, 10-mm slice thickness, midventricular short-axis slice	75	Age range 20–90 y (56 ± 19 y), 53% men	24 ± 5, range 12–33 (global); 25 ± 5, range 11–39 (septum)

nonischemic cardiomyopathy). Some diseases alter parametric values globally, whereas others have regional effects.

In general, native T1 and ECV values are increased when the extracellular space is expanded, such as in the setting of myocardial fibrosis, edema, or amyloid. Native T1 values are decreased in the setting of iron, fat, Fabry disease, and hemorrhage.

Water increases the T2 relaxation time of tissues, and therefore myocardial T2 values are increased in the setting of edema, inflammation, and acute ischemia [30,31]. Myocardial T2 and T2* values are decreased in the setting of iron and hemorrhage [32].

According to recent guidelines, parametric mapping provides unique information to guide clinical care and should be applied in the setting of potential myocarditis, iron overload, amyloid, and Fabry disease [17]. Parametric mapping techniques have potential clinical utility in multiple other scenarios, including cardiomyopathies, acute and chronic myocardial infarction, and athlete's heart.

Given that absolute parametric mapping values vary depending on the specific technique used, cutoff values for specific diseases reported in individual studies should not be universally applied in clinical practice. Parametric mapping results should be evaluated against local reference ranges, generated from data sets that were acquired, processed, and analyzed in the same way as the desired clinical application [17].

Myocardial fibrosis

Myocardial fibrosis is a common and final pathway in multiple cardiomyopathies, and is associated with adverse cardiac outcomes, including diastolic and

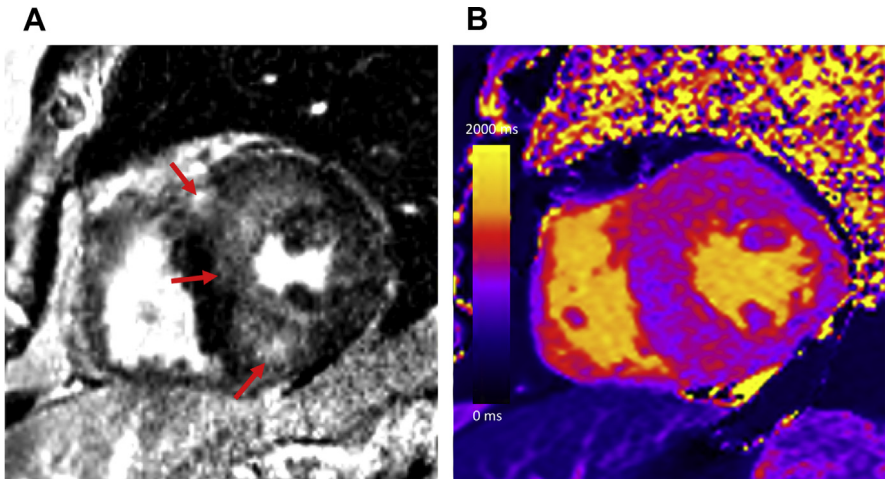

FIG. 1 A 52-year-old man with gene-positive HCM. (**A**) Midventricular short-axis LGE image shows asymmetric septal left ventricular hypertrophy and patchy, predominantly midwall LGE involving the right ventricular insertion points, anterior wall, and septum (*arrows*). (**B**) Midventricular short-axis native T1 map (1.5 T) shows moderately increased T1 values in areas with LGE (septum, 1102 milliseconds) and mildly increased global native T1 values remote from areas of LGE (lateral wall, 980 milliseconds). Global myocardial ECV was also mildly increased (30%, not shown).

systolic heart failure [33]. Increased native T1 and ECV values have been shown to correlate with histologic markers of myocardial fibrosis in multiple diseases, including hypertrophic cardiomyopathy (HCM), dilated cardiomyopathy (DCM), and aortic stenosis [34].

Hypertrophic cardiomyopathy. HCM is the most common cause of sudden cardiac death in young adults. Cardiac MRI plays an important role in the detection of left ventricular hypertrophy and LGE in patients with HCM [35]. Native T1 and ECV values are diffusely increased in HCM, even in segments without LGE (Fig. 1) [36]. Native T1 and ECV have been shown to reflect fibrosis on histology [37,38]. Increased native T1 values correlate with increased wall thickness, suggesting that it is a marker of disease severity [39,40].

Dilated cardiomyopathy. Nonischemic idiopathic DCM is characterized by left ventricular dilatation and systolic dysfunction without an obvious or detectable underlying cause [41]. The classic pattern of LGE in DCM is linear midwall, although many patients do not show LGE [42]. Native T1 and ECV values are slightly increased in patients with DCM, and correlate with functional left ventricular parameters such as ejection fraction and strain (Fig. 2) [40,43–46]. ECV has been shown to correlate with myocardial collagen content based on histology in patients with DCM [44]. Myocardial T2 values may also be mildly increased in DCM, suggesting edema [46–48].

Aortic stenosis. In patients with severe aortic stenosis, the degree of left ventricular hypertrophy is independently associated with higher rates of cardiovascular events [49]. Patients with aortic stenosis have increased native T1 and ECV values, which have been shown to correlate with the degree of histologic interstitial fibrosis [50,51].

Myocardial edema

Intramyocardial water is normally distributed within intracellular and intravascular spaces [4]. Myocardial injury alters this balance, resulting in cytotoxic edema (intracellular fluid accumulation) or vasogenic edema (interstitial fluid accumulation), depending on the type of injury. Edema is an important manifestation of acute heart disease, including ischemic causes (such as myocardial infarction) and nonischemic causes (such as myocarditis, stress-induced cardiomyopathy, and cardiac transplant rejection).

Myocardial ischemia and infarction. Increased myocardial T1, T2, and ECV values have been shown in acute and chronic myocardial infarction [52–55]. In the setting of acute myocardial infarction, the area at

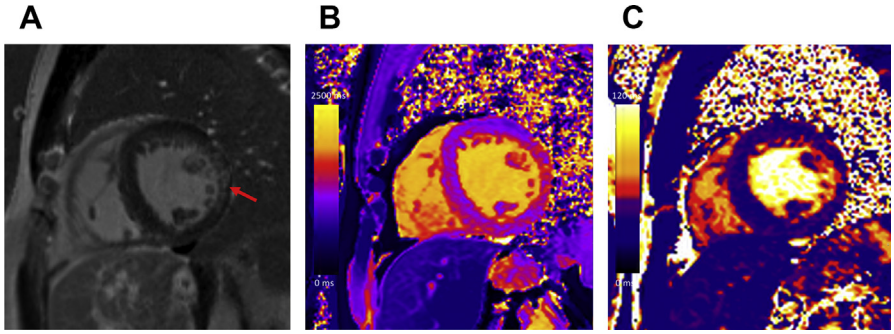

FIG. 2 A 51-year-old woman with idiopathic DCM. (**A**) Midventricular short-axis LGE image shows mild-intensity midwall LGE at the lateral wall (*arrow*). (**B**) Midventricular short-axis native T1 map (3.0 T) shows globally mildly increased native T1 values (1315 milliseconds) and moderately increased native T1 values corresponding with the area of LGE (1407 milliseconds). (**C**) Midventricular short-axis native T2 map (3.0 T) shows no evidence of myocardial T2 increase (40 milliseconds).

risk (AAR) represents the entire myocardial perfusion bed distal to an occluded coronary artery, including necrotic nonviable core (infarction) and surrounding potentially salvageable viable zone (ischemia). Native T1 and T2 may be useful in quantifying the AAR and evaluating myocardial salvage in reperfused patients with acute ST-segment elevation myocardial infarction (STEMI) [55–57]. Native T1 mapping may be superior to T2-weighted imaging in detecting areas of injury in patients with non–ST-segment elevation myocardial infarction [58]. In the acute setting, elevated native T1, T2 and ECV values have been described in myocardium remote from the infarction, suggesting edema outside the AAR and possibly early remodeling [59–62]. Native T1 values remote from the infarct are independently predictive of adverse cardiac events in patients with reperfused STEMI [60].

T1 and T2 mapping may be used to identify adverse prognostic features in acute myocardial infarction, including microvascular obstruction and intramyocardial hemorrhage [63–65]. T2* values are relatively insensitive to edema, and may be more suitable than T2 values to detect myocardial hemorrhage after reperfusion in patients with acute myocardial infarction [65,66].

In the setting of chronic infarction, native T1 and ECV values are increased compared with normal myocardium; however, values are lower and less extensive compared with acute infarction [54]. Native T1 mapping is able to identify areas of lipomatous metaplasia in chronic infarction due to very low T1 values [67]. More recently, native T1 mapping with pharmacologic stress has been shown to detect and differentiate between obstructive epicardial coronary artery disease and microvascular dysfunction [68].

Nonischemic myocardial edema. T1 and T2 mapping have been shown to detect myocardial edema in several other diseases, including myocarditis, stress-induced (Takotsubo) cardiomyopathy, cardiac sarcoidosis, and cardiac transplant rejection [69–72]. Several studies have shown superior diagnostic performance of parametric mapping techniques compared with T2-weighted imaging for detection of myocardial edema [55,72].

T1, T2, and ECV values have clinical utility in the evaluation of suspected myocarditis [73,74]. Parametric mapping improves the diagnostic performance of cardiac MRI for detection of acute myocarditis compared with conventional imaging findings such as T2-weighted hyperintensity, early gadolinium enhancement, and LGE [75]. Native T1 and T2 are also useful in discriminating between acute and convalescent phases of myocarditis [75]. In acute myocarditis, abnormal myocardial edema detected on T1 and T2 maps typically colocalizes with regions of LGE because of associated cellular destruction (Fig. 3).

Native T1, T2, and ECV values are also increased in the setting of acute cardiac transplant rejection [69,76,77]. Implementation of parametric mapping after cardiac transplant could potentially reduce the number of routine serial endomyocardial biopsies performed for rejection surveillance [76].

Native T1 and T2 values are also increased in myocardial segments with wall motion abnormalities in patients with stress-induced cardiomyopathy

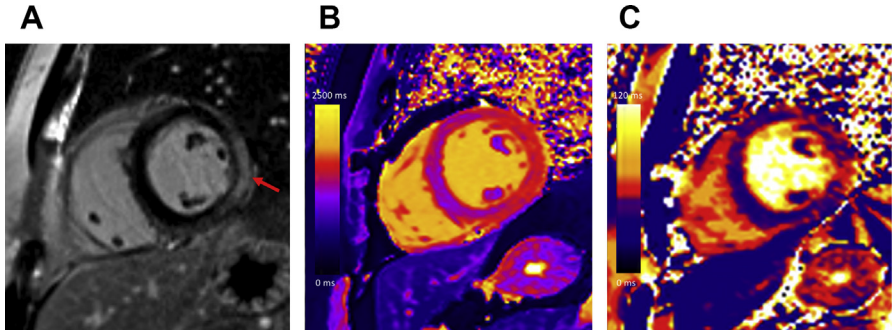

FIG. 3 A 31-year-old man with acute viral myocarditis. (**A**) Midventricular short-axis LGE image shows subepicardial LGE at the inferior lateral wall (*arrow*). (**B**) Midventricular short-axis native T1 map (3.0 T) shows increased T1 values corresponding with the area of LGE (1484 milliseconds). (**C**) Midventricular short-axis native T2 map (3.0 T) shows increased T2 values corresponding with the area of LGE (53 milliseconds).

(Fig. 4) [71,78]. Parametric values improve on follow-up; however, persistent long-term myocardial changes have been described [78].

Cardiac amyloid

Amyloidosis is a group of diseases in which misfolded or misassembled proteins accumulate in the extracellular space of organs, including the heart. Light chain (AL) and transthyretin (ATTR) are the most common types of amyloid that involve the heart. Patients with cardiac amyloid typically present with a restrictive cardiomyopathy with atrial dilatation and concentric ventricular hypertrophy [79]. Early detection is critical because cardiac amyloid portends a poor prognosis and treatment is dictated by the type and degree of cardiac involvement. Classic LGE cardiac MRI findings include dark blood pool, difficulty nulling the myocardium, and subendocardial to diffuse myocardial enhancement [80]. Native T1 and ECV values are dramatically increased in cardiac amyloid, because of expansion of the interstitial space from fibrillar deposits, and have been shown to predict mortality (Fig. 5) [81–85]. In contrast, myocardial T2 values are not increased in cardiac amyloid [85,86]. Native T1 and ECV values differ between subtypes: native T1 is higher in AL, whereas ECV is higher in ATTR [81,87]. Native T1 and ECV may be useful in guiding and monitoring response to therapy in patients with cardiac amyloid [88].

Fabry disease

Fabry disease is an X-linked disorder characterized by progressive lysosomal sphingolipid accumulation in multiple organs, including the heart [89]. Cardiac MRI

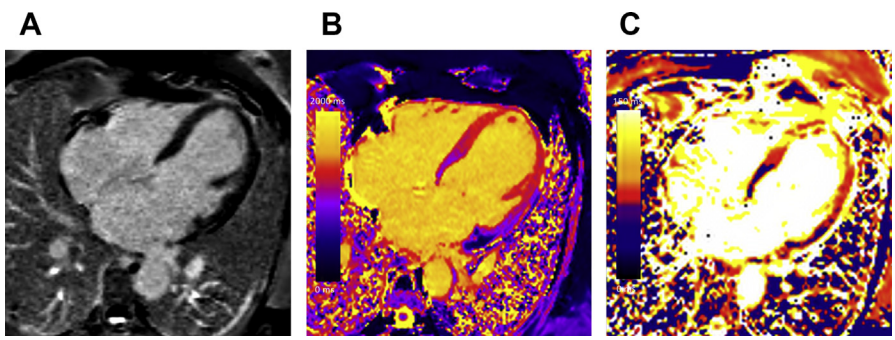

FIG. 4 A 63-year-old woman with stress-induced (Takotsubo) cardiomyopathy with apical ballooning in systole (not shown). (**A**) Four-chamber LGE image shows no myocardial LGE. (**B**) Four-chamber native T1 map (1.5 T) shows severely increased T1 values at the apex (1345 milliseconds), corresponding with the area of wall motion abnormality. (**C**) Four-chamber native T2 map (1.5 T) also shows severely increased T2 values at the apex (92 milliseconds).

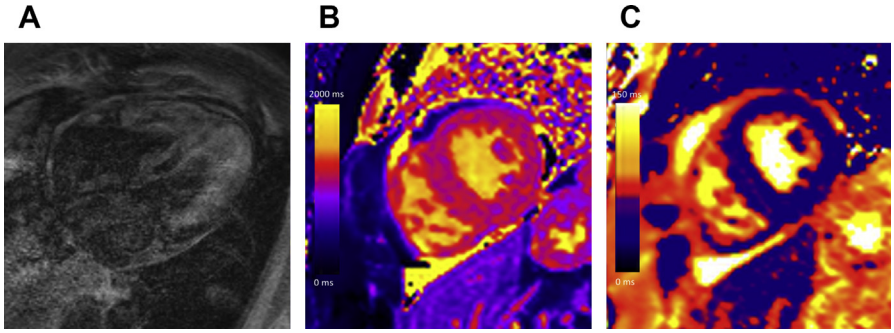

FIG. 5 A 68-year-old woman with cardiac amyloid. (**A**) Four-chamber LGE image shows dark blood pool and diffuse biventricular and biatrial LGE. (**B**) Midventricular short-axis native T1 map (1.5 T) shows severely increased global T1 values (1201 milliseconds). (**C**) Midventricular short-axis native T2 map (1.5 T) shows no evidence of T2 increase (50 milliseconds).

plays an important role in patients with Fabry disease, including assessment of left ventricular hypertrophy, maximum left ventricular wall thickness, and LGE. The classic pattern of LGE in Fabry disease is midwall involving the basal inferior lateral segment, although this pattern is not seen in all patients [90]. Native T1 is significantly lower in patients with Fabry disease compared with normal controls and patients with HCM, likely reflecting myocardial glycosphingolipid deposition (Fig. 6) [91–94]. ECV is typically within the normal range in patients with Fabry disease [93,94]. Native T2 values are increased in areas of LGE, possibly reflecting inflammation [95,96].

Iron overload

Cardiac iron overload resulting from altered iron hemostasis, increased intestinal absorption, and chronic transfusions is associated with adverse outcomes, including heart failure and arrhythmia. Iron overload may be reversible if chelation therapy is instituted early, therefore timely identification is imperative. Cardiac iron concentration is inversely related to T1, T2, and T2* values (Fig. 7). Cardiac MRI T2* analysis is the clinical standard for noninvasive assessment of myocardial iron, and has been validated based on histology with high sensitivity and reproducibility [27,97]. Midseptal T2* values less than 20 milliseconds are considered clinically important, whereas values less than 10 milliseconds are considered evidence of severe iron overload [98].

Native T1 may be more sensitive and reproducible than T2* in the evaluation of myocardial iron, particularly in the setting of severe and mild iron overload in which T2* analysis is less reliable [99,100]. ECV is increased in patients with myocardial iron overload, possibly reflecting interstitial fibrosis [101].

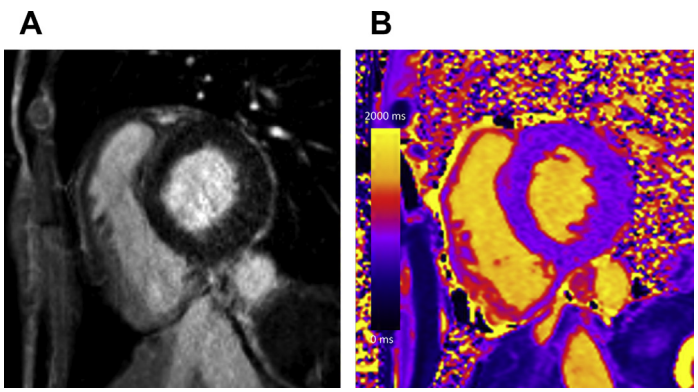

FIG. 6 A 39-year-old man with gene-positive Fabry disease. (**A**) Basal short-axis LGE image shows no LGE. (**B**) Midventricular short-axis native T1 map (1.5 T) shows low global native T1 values (879 milliseconds).

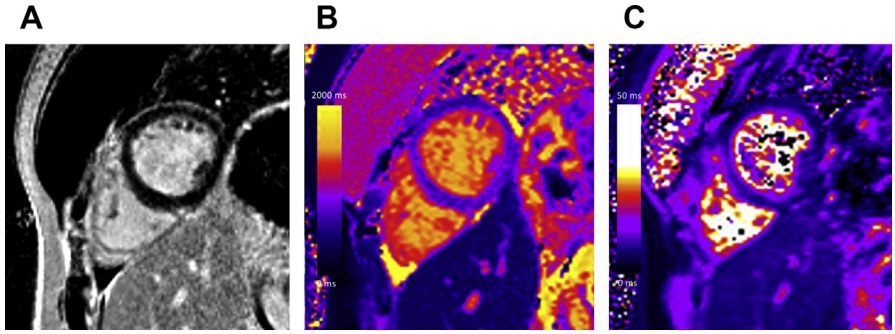

FIG. 7 A 24-year-old woman with β-thalassemia major and cardiac iron overload. (**A**) Midventricular short-axis LGE image shows no evidence of LGE. (**B**) Midventricular short-axis native T1 map (1.5 T) shows low global native T1 values (759 milliseconds). (**C**) Midventricular short-axis T2* map (1.5 T) shows low global T2* values, in keeping with iron overload (15 milliseconds).

Other diseases

ECV may be helpful in distinguishing between athlete's heart and HCM. In the setting of athlete's heart, ECV is reduced with increasing left ventricular mass because of expansion of the cellular component and decrease in the extracellular volume [36,102]. In contrast, in patients with HCM, ECV is increased with increasing left ventricular mass because of extracellular matrix expansion.

Native T1 and T2 values are increased in patients with cardiac sarcoidosis [30,70]. Values improve following treatment, suggesting that parametric mapping may be helpful in monitoring response to therapy [30,70].

T1, T2, and ECV are helpful in identifying myocardial involvement in systemic inflammatory disorders such as systemic lupus erythematosus and rheumatoid arthritis [103–105].

Increased T1 and ECV values have also been reported in patients with congenital heart disease, including tetralogy of Fallot [106,107].

PRESENT RELEVANCE AND FUTURE AVENUES

Cardiac MRI parametric mapping techniques provide complementary and incremental information beyond qualitative techniques in the evaluation of myocardial diseases. Current evidence supports clinical implementation of parametric mapping in several diseases, including amyloid, myocarditis, iron overload, and Fabry disease. Future research may show the value of parametric mapping for risk classification and risk modification by guiding therapy in different diseases.

SUMMARY

T1, T2, and T2* mapping techniques are useful in the evaluation of patients with several different diseases, potentially aiding in narrowing the differential diagnosis, monitoring response to treatment, and providing prognostic information.

REFERENCES

[1] Lorenz CH, Walker ES, Morgan VL, et al. Normal human right and left ventricular mass, systolic function, and gender differences by cine magnetic resonance imaging. J Cardiovasc Magn Reson 1999;1:7–21.
[2] Roujol S, Weingärtner S, Foppa M, et al. Accuracy, precision, and reproducibility of four T1 mapping sequences: a head-to-head comparison of MOLLI, ShMOLLI, SASHA, and SAPPHIRE. Radiology 2014; 272:683–9.
[3] Radenkovic D, Weingärtner S, Ricketts L, et al. T1mapping in cardiac MRI. Heart Fail Rev 2017;22:415–30.
[4] Taylor AJ, Salerno M, Dharmakumar R, et al. T1 mapping basic techniques and clinical applications. JACC Cardiovasc Imaging 2016;9:67–81.
[5] Aus dem Siepen F, Baumgärtner C, Müller-Henessen M, et al. Variability of cardiovascular magnetic resonance (CMR) T1 mapping parameters in healthy volunteers during long-term follow-up. Open Heart 2018;5: e000717.
[6] Arheden H, Saeed M, Higgins CB, et al. Measurement of the distribution volume of gadopentetate dimeglumine at echo-planar MR imaging to quantify myocardial infarction: comparison with 99m Tc-DTPA autoradiography in rats. Radiology 1999;211:698–708.
[7] Robison S, Karur GR, Wald RM, et al. Noninvasive hematocrit assessment for cardiovascular magnetic resonance extracellular volume quantification using a

point-of-care device and synthetic derivation. J Cardiovasc Magn Reson 2018;20:1–9.
[8] Treibel TA, Fontana M, Maestrini V, et al. Automatic measurement of the myocardial interstitium synthetic extracellular volume quantification without hematocrit sampling. JACC Cardiovasc Imaging 2016;9:54–63.
[9] Engblom H, Kanski M, Kopic S, et al. Importance of standardizing timing of hematocrit measurement when using cardiovascular magnetic resonance to calculate myocardial extracellular volume (ECV) based on pre- and post-contrast T1 mapping. J Cardiovasc Magn Reson 2018;20:46.
[10] Messroghli DR, Plein S, Higgins DM, et al. Human myocardium: single-breath-hold MR T1 mapping with high spatial resolution—reproducibility study. Radiology 2006;238:1004–12.
[11] Roy C, Slimani A, De Meester C, et al. Age and sex corrected normal reference values of T1, T2 T2*and ECV in healthy subjects at 3T CMR. J Cardiovasc Magn Reson 2017;19:72.
[12] Kawel N, Nacif M, Zavodni A, et al. T1 mapping of the myocardium: intra-individual assessment of post-contrast T1 time evolution and extracellular volume fraction at 3T for Gd-DTPA and Gd-BOPTA. J Cardiovasc Magn Reson 2012;14:26.
[13] Stanisz GJ, Odrobina EE, Pun J, et al. T1, T2 relaxation and magnetization transfer in tissue at 3T. Magn Reson Med 2005;54:507–12.
[14] Teixeira T, Hafyane T, Stikov N, et al. Comparison of different cardiovascular magnetic resonance sequences for native myocardial T1 mapping at 3T. J Cardiovasc Magn Reson 2016;18:1–12.
[15] Von Knobelsdorff-Brenkenhoff F, Prothmann M, Dieringer MA, et al. Myocardial T1 and T2 mapping at 3 T: reference values, influencing factors and implications. J Cardiovasc Magn Reson 2013;15:53.
[16] Rauhalammi SMO, Mangion K, Barrientos PH, et al. Native myocardial longitudinal (T1) relaxation time: regional, age, and sex associations in the healthy adult heart. J Magn Reson Imaging 2016;44:541–8.
[17] Messroghli DR, Moon JC, Ferreira VM, et al. Clinical recommendations for cardiovascular magnetic resonance mapping of T1, T2, T2 and extracellular volume: a consensus statement by the Society for Cardiovascular Magnetic Resonance (SCMR) endorsed by the European Association for Cardiovascular Imaging. J Cardiovasc Magn Reson 2017;19:75.
[18] Moon JC, Messroghli DR, Kellman P, et al. Myocardial T1 mapping and extracellular volume quantification: a Society for Cardiovascular Magnetic Resonance (SCMR) and CMR Working Group of the European Society of Cardiology consensus statement. J Cardiovasc Magn Reson 2013;15:92.
[19] Sado DM, Flett AS, Banypersad SM, et al. Cardiovascular magnetic resonance measurement of myocardial extracellular volume in health and disease. Heart 2012;98:1436–41.
[20] Kellman P, Arai AE, Xue H. T1 and extracellular volume mapping in the heart: estimation of error maps and the influence of noise on precision. J Cardiovasc Magn Reson 2013;15:56.
[21] Wassmuth R, Prothmann M, Utz W, et al. Variability and homogeneity of cardiovascular magnetic resonance myocardial T2-mapping in volunteers compared to patients with edema. J Cardiovasc Magn Reson 2013;15:27.
[22] Huang TY, Liu YJ, Stemmer A, et al. T2 measurement of the human myocardium using a T 2-prepared transient-state trueFISP sequence. Magn Reson Med 2007;57:960–6.
[23] Giri S, Chung YC, Merchant A, et al. T2 quantification for improved detection of myocardial edema. J Cardiovasc Magn Reson 2009;11:56.
[24] Baeßler B, Schaarschmidt F, Stehning C, et al. A systematic evaluation of three different cardiac T2-mapping sequences at 1.5 and 3T in healthy volunteers. Eur J Radiol 2015;84:2161–70.
[25] Bönner F, Janzarik N, Jacoby C, et al. Myocardial T2 mapping reveals age- and sex-related differences in volunteers. J Cardiovasc Magn Reson 2015;17:9.
[26] Gillis P, Roch A, Brooks RA. Corrected equations for susceptibility-induced T2-Shortening. J Magn Reson 1999;137:402–7.
[27] Kirk P, He T, Anderson LJ, et al. International reproducibility of single breathhold T2* MR for cardiac and liver iron assessment among five thalassemia centers. J Magn Reson Imaging 2010;32:315–9.
[28] Smith GC, Carpenter JP, He T, et al. Value of black blood T2* cardiovascular magnetic resonance. J Cardiovasc Magn Reson 2011;13:21.
[29] Pennell DJ, Udelson JE, Arai AE, et al. Cardiovascular function and treatment in β-thalassemia major: a consensus statement from the American Heart Association. Circulation 2013;128:281–308.
[30] Puntmann VO, Isted A, Hinojar R, et al. T1 and T2 mapping in recognition of early cardiac involvement in systemic sarcoidosis. Radiology 2017;285:63–72.
[31] Spieker M, Haberkorn S, Gastl M, et al. Abnormal T2 mapping cardiovascular magnetic resonance correlates with adverse clinical outcome in patients with suspected acute myocarditis. J Cardiovasc Magn Reson 2017;19:38.
[32] Captur G, Manisty C, Moon JC. Cardiac MRI evaluation of myocardial disease. Heart 2016;102:1429–35.
[33] Schelbert EB, Piehler KM, Zareba KM, et al. Myocardial fibrosis quantified by extracellular volume is associated with subsequent hospitalization for heart failure, death, or both across the spectrum of ejection fraction and heart failure stage. J Am Heart Assoc 2015;4:e002613.
[34] Diao K, Yang Z, Xu H, et al. Histologic validation of myocardial fibrosis measured by T1 mapping: a systematic review and meta-analysis. J Cardiovasc Magn Reson 2016;18:92.

[35] Maron MS, Maron BJ, Harrigan C, et al. Hypertrophic cardiomyopathy phenotype revisited after 50 years with cardiovascular magnetic resonance. J Am Coll Cardiol 2009;54:220–8.
[36] Swoboda PP, McDiarmid AK, Erhayiem B, et al. Assessing myocardial extracellular volume by T1 mapping to distinguish hypertrophic cardiomyopathy from athlete's heart. J Am Coll Cardiol 2016;67:2189–90.
[37] Ellims AH, Iles LM, Ling LH, et al. A comprehensive evaluation of myocardial fibrosis in hypertrophic cardiomyopathy with cardiac magnetic resonance imaging: linking genotype with fibrotic phenotype. Eur Heart J Cardiovasc Imaging 2014;15:1108–16.
[38] Flett AS, Hayward MP, Ashworth MT, et al. Equilibrium contrast cardiovascular magnetic resonance for the measurement of diffuse myocardial fibrosis: preliminary validation in humans. Circulation 2010;122:138–44.
[39] Puntmann VO, Voigt T, Chen Z, et al. Native T1 mapping in differentiation of normal myocardium from diffuse disease in hypertrophic and dilated cardiomyopathy. JACC Cardiovasc Imaging 2013;6:475–84.
[40] Dass S, Suttie JJ, Piechnik SK, et al. Myocardial tissue characterization using magnetic resonance noncontrast T1 mapping in hypertrophic and dilated cardiomyopathy. Circ Cardiovasc Imaging 2012;5:726–33.
[41] Maron BJ, Towbin JA, Thiene G, et al. Contemporary definitions and classification of the cardiomyopathies: An American Heart Association Scientific Statement from the Council on Clinical Cardiology, Heart Failure and Transplantation Committee; Quality of Care and Outcomes Research and Functional Genomics and Translational Biology Interdisciplinary Working Groups; and Council on Epidemiology and Prevention. Circulation 2006;113:1807–16.
[42] Assomull RG, Prasad SK, Lyne J, et al. Cardiovascular magnetic resonance, fibrosis, and prognosis in dilated cardiomyopathy. J Am Coll Cardiol 2006;48:1977–85.
[43] Hong YJ, Park CH, Kim YJ, et al. Extracellular volume fraction in dilated cardiomyopathy patients without obvious late gadolinium enhancement: comparison with healthy control subjects. Int J Cardiovasc Imaging 2015;31:115–22.
[44] aus dem Siepen F, Buss SJ, Messroghli D, et al. T1 mapping in dilated cardiomyopathy with cardiac magnetic resonance: quantification of diffuse myocardial fibrosis and comparison with endomyocardial biopsy. Eur Heart J Cardiovasc Imaging 2015;16:210–6.
[45] Puntmann VO, Ucar EA, Baydes RH, et al. Aortic stiffness and interstitial myocardial fibrosis by native t1 are independently associated with left ventricular remodeling in patients with dilated cardiomyopathy. Hypertension 2014;64:762–8.
[46] Mordi I, Carrick D, Bezerra H, et al. T1and T2mapping for early diagnosis of dilated non-ischaemic cardiomyopathy in middle-aged patients and differentiation from normal physiological adaptation. Eur Heart J Cardiovasc Imaging 2016;17:797–803.
[47] He T, Gulati A, Jabbour A, et al. Cardiovascular magnetic resonance T2 mapping detects myocardial edema in patients with chronic dilated cardiomyopathy. J Cardiovasc Magn Reson 2012;14:O29.
[48] Jeserich M, Föll D, Olschewski M, et al. Evidence of myocardial edema in patients with nonischemic dilated cardiomyopathy. Clin Cardiol 2012;35:371–6.
[49] Cioffi G, Faggiano P, Vizzardi E, et al. Prognostic effect of inappropriately high left ventricular mass in asymptomatic severe aortic stenosis. Heart 2011;97:301–7.
[50] Lee S-P, Lee W, Lee JM, et al. Assessment of diffuse myocardial fibrosis by using MR imaging in asymptomatic patients with aortic stenosis. Radiology 2015;274:359–69.
[51] White SK, Sado DM, Fontana M, et al. T1 mapping for myocardial extracellular volume measurement by CMR: bolus only versus primed infusion technique. JACC Cardiovasc Imaging 2013;6:955–62.
[52] Messroghli DR, Walters K, Plein S, et al. Myocardial T1 mapping: application to patients with acute and chronic myocardial infarction. Magn Reson Med 2007;58:34–40.
[53] Dall'Armellina E, Ferreira VM, Kharbanda RK, et al. Diagnostic value of pre-contrast T1 mapping in acute and chronic myocardial infarction. JACC Cardiovasc Imaging 2013;6:739–42.
[54] Ugander M, Oki AJ, Hsu LY, et al. Extracellular volume imaging by magnetic resonance imaging provides insights into overt and sub-clinical myocardial pathology. Eur Heart J 2012;33:1268–78.
[55] Verhaert D, Thavendiranathan P, Giri S, et al. Direct T2 quantification of myocardial edema in acute ischemic injury. JACC Cardiovasc Imaging 2011;4:269–78.
[56] Ugander M, Bagi PS, Oki AJ, et al. Myocardial edema as detected by pre-contrast T1 and T2 CMR delineates area at risk associated with acute myocardial infarction. JACC Cardiovasc Imaging 2012;5:596–603.
[57] Bulluck H, White SK, Rosmini S, et al. T1 mapping and T2 mapping at 3T for quantifying the area-at-risk in reperfused STEMI patients. J Cardiovasc Magn Reson 2015;17:73.
[58] Dall'Armellina E, Piechnik SK, Ferreira VM, et al. Cardiovascular magnetic resonance by non contrast T1-mapping allows assessment of severity of injury in acute myocardial infarction. J Cardiovasc Magn Reson 2012;14:15.
[59] Manrique A, Gerbaud E, Derumeaux G, et al. Cardiac magnetic resonance demonstrates myocardial oedema in remote tissue early after reperfused myocardial infarction. Arch Cardiovasc Dis 2009;102:633–9.
[60] Carrick D, Haig C, Rauhalammi S, et al. Pathophysiology of LV remodeling in survivors of STEMI inflammation, remote myocardium, and prognosis. JACC Cardiovasc Imaging 2015;8:779–89.
[61] Chan W, Duffy SJ, White DA, et al. Acute left ventricular remodeling following myocardial infarction: coupling

of regional healing with remote extracellular matrix expansion. JACC Cardiovasc Imaging 2012;5:884–93.
[62] Carberry J, Carrick D, Haig C, et al. Remote zone extracellular volume and left ventricular remodeling in survivors of ST-elevation myocardial infarction. Hypertension 2016;68:385–91.
[63] Carrick D, Haig C, Rauhalammi S, et al. Prognostic significance of infarct core pathology revealed by quantitative non-contrast in comparison with contrast cardiac magnetic resonance imaging in reperfused ST-elevation myocardial infarction survivors. Eur Heart J 2016;37:1044–59.
[64] Pedersen SF, Thrysøe SA, Robich MP, et al. Assessment of intramyocardial hemorrhage by T1-weighted cardiovascular magnetic resonance in reperfused acute myocardial infarction. J Cardiovasc Magn Reson 2012;14:59.
[65] Zia MI, Ghugre NR, Connelly KA, et al. Characterizing myocardial edema and hemorrhage using quantitative T2 and T2* mapping at multiple time intervals post ST-segment elevation myocardial infarction. Circ Cardiovasc Imaging 2012;5:566–72.
[66] Kali A, Tang RL, Kumar A, et al. Detection of acute reperfusion myocardial hemorrhage with cardiac MR imaging: T2 versus T2. Radiology 2013;269:387–95.
[67] O H-Ici D, Jeuthe S, Al-Wakeel N, et al. T1 mapping in ischaemic heart disease. Eur Heart J Cardiovasc Imaging 2014;15:597–602.
[68] Liu A, Wijesurendra RS, Liu JM, et al. Gadolinium-free cardiac MR stress T1-mapping to distinguish epicardial from microvascular coronary disease. J Am Coll Cardiol 2018;71:957–68.
[69] Usman AA, Taimen K, Wasielewski M, et al. Cardiac magnetic resonance T2 mapping in the monitoring and follow-up of acute cardiac transplant rejection: a pilot study. Circ Cardiovasc Imaging 2012;5:782–90.
[70] Crouser ED, Ono C, Tran T, et al. Improved detection of cardiac sarcoidosis using magnetic resonance with myocardial T2 mapping. Am J Respir Crit Care Med 2014;189:109–12.
[71] Thavendiranathan P, Walls M, Giri S, et al. Improved detection of myocardial involvement in acute inflammatory cardiomyopathies using T2 mapping. Circ Cardiovasc Imaging 2012;5:102–10.
[72] Ferreira VM, Piechnik SK, Dall'Armellina E, et al. T1 Mapping for the diagnosis of acute myocarditis using CMR: comparison to T2-Weighted and late gadolinium enhanced imaging. JACC Cardiovasc Imaging 2013;6:1048–58.
[73] Lurz P, Luecke C, Eitel I, et al. Comprehensive cardiac magnetic resonance imaging in patients with suspected myocarditis the MyoRacer-trial. J Am Coll Cardiol 2016;67:1800–11.
[74] Ferreira VM, Piechnik SK, Dall'Armellina E, et al. Native T1-mapping detects the location, extent and patterns of acute myocarditis without the need for gadolinium contrast agents. J Cardiovasc Magn Reson 2014;16:36.
[75] Luetkens JA, Homsi R, Sprinkart AM, et al. Incremental value of quantitative CMR including parametric mapping for the diagnosis of acute myocarditis. Eur Heart J Cardiovasc Imaging 2016;17:154–61.
[76] Vermes E, Pantaléon C, Auvet A, et al. Cardiovascular magnetic resonance in heart transplant patients: diagnostic value of quantitative tissue markers: T2 mapping and extracellular volume fraction, for acute rejection diagnosis. J Cardiovasc Magn Reson 2018;20:59.
[77] Miller CA, Naish JH, Shaw SM, et al. Multiparametric cardiovascular magnetic resonance surveillance of acute cardiac allograft rejection and characterisation of transplantation-associated myocardial injury: a pilot study. J Cardiovasc Magn Reson 2014;16:52.
[78] Scally C, Rudd A, Mezincescu A, et al. Persistent long-term structural, functional, and metabolic changes after stress-induced (Takotsubo) cardiomyopathy. Circulation 2018;137:1039–48.
[79] Banypersad SM, Moon JC, Whelan C, et al. Updates in cardiac amyloidosis: a review. J Am Heart Assoc 2012;1:e000364.
[80] Maceira AM, Joshi J, Prasad SK, et al. Cardiovascular magnetic resonance in cardiac amyloidosis. Circulation 2005;111:186–93.
[81] Fontana M, Banypersad SM, Treibel TA, et al. Native T1 mapping in transthyretin amyloidosis. JACC Cardiovasc Imaging 2014;7:157–65.
[82] Karamitsos TD, Piechnik SK, Banypersad SM, et al. Noncontrast T1 mapping for the diagnosis of cardiac amyloidosis. JACC Cardiovasc Imaging 2013;6:488–97.
[83] Bull S, White SK, Piechnik SK, et al. Human non-contrast T1 values and correlation with histology in diffuse fibrosis. Heart 2013;99:932–7.
[84] Brooks J, Kramer CM, Salerno M. Markedly increased volume of distribution of gadolinium in cardiac amyloidosis demonstrated by T1 mapping. J Magn Reson Imaging 2013;38:1591–5.
[85] Banypersad SM, Fontana M, Maestrini V, et al. T1 mapping and survival in systemic light-chain amyloidosis. Eur Heart J 2015;36(4):244–51.
[86] Sparrow P, Amirabadi A, Sussman MS, et al. Quantitative assessment of myocardial T2 relaxation times in cardiac amyloidosis. J Magn Reson Imaging 2009;30:942–6.
[87] Fontana M, Banypersad SM, Treibel TA, et al. Differential myocyte responses in patients with cardiac transthyretin amyloidosis and light-chain amyloidosis: a cardiac MR imaging study. Radiology 2015;277:388–97.
[88] Richards DB, Cookson LM, Berges AC, et al. Therapeutic clearance of amyloid by antibodies to serum amyloid P component. N Engl J Med 2015;373:1106–14.
[89] Clarke JTR. Narrative review: Fabry disease. Ann Intern Med 2007;146:425–33.
[90] Deva DP, Hanneman K, Li Q, et al. Cardiovascular magnetic resonance demonstration of the spectrum of morphological phenotypes and patterns of myocardial

scarring in Anderson-Fabry disease. J Cardiovasc Magn Reson 2016;18:14.
[91] Thompson RB, Chow K, Khan A, et al. T1mapping with cardiovascular MRI is highly sensitive for Fabry disease independent of hypertrophy and sex. Circ Cardiovasc Imaging 2013;6:637–45.
[92] Sado DM, White SK, Piechnik SK, et al. Identification and assessment of Anderson-Fabry disease by cardiovascular magnetic resonance noncontrast myocardial T1 mapping. Circ Cardiovasc Imaging 2013;6:392–8.
[93] Pica S, Sado DM, Maestrini V, et al. Reproducibility of native myocardial T1 mapping in the assessment of Fabry disease and its role in early detection of cardiac involvement by cardiovascular magnetic resonance. J Cardiovasc Magn Reson 2014;16:99.
[94] Karur GR, Robison S, Iwanochko RM, et al. Use of myocardial T1 mapping at 3.0 t to differentiate Anderson-Fabry disease from hypertrophic cardiomyopathy. Radiology 2018;288:398–406.
[95] Nordin S, Kozor R, Bulluck H, et al. Cardiac Fabry disease with late gadolinium enhancement is a chronic inflammatory cardiomyopathy. J Am Coll Cardiol 2016;15:1707–8.
[96] Nordin S, Kozor R, Baig S, et al. Cardiac phenotype of prehypertrophic Fabry disease. Circ Cardiovasc Imaging 2018;11:e007168.
[97] Carpenter JP, He T, Kirk P, et al. On T2* magnetic resonance and cardiac iron. Circulation 2011;123:1519–28.
[98] Kirk P, Roughton M, Porter JB, et al. Cardiac T2* magnetic resonance for prediction of cardiac complications in Thalassemia Major. Circulation 2009;120:1961–8.
[99] Sado DM, Maestrini V, Piechnik SK, et al. Noncontrast myocardial T1 mapping using cardiovascular magnetic resonance for iron overload. J Magn Reson Imaging 2015;41:1505–11.
[100] Alam MH, Auger D, Smith GC, et al. T1 at 1.5T and 3T compared with conventional T2* at 1.5T for cardiac siderosis. J Cardiovasc Magn Reson 2015;17:102.
[101] Hanneman K, Nguyen ET, Thavendiranathan P, et al. Quantification of myocardial extracellular volume fraction with cardiac MR imaging in Thalassemia major. Radiology 2016;279:720–30.
[102] McDiarmid AK, Swoboda PP, Erhayiem B, et al. Athletic cardiac adaptation in males is a consequence of elevated myocyte mass. Circ Cardiovasc Imaging 2016;9:e003579.
[103] Hinojar R, Foote L, Sangle S, et al. Native T1 and T2 mapping by CMR in lupus myocarditis: disease recognition and response to treatment. Int J Cardiol 2016;222:717–26.
[104] Greulich S, Mayr A, Kitterer D, et al. Advanced myocardial tissue characterisation by a multi-component CMR protocol in patients with rheumatoid arthritis. Eur Radiol 2017;27:4639–49.
[105] Ntusi NAB, Piechnik SK, Francis JM, et al. Diffuse myocardial fibrosis and inflammation in rheumatoid arthritis: insights from CMR T1 Mapping. JACC Cardiovasc Imaging 2015;8:526–36.
[106] Hanneman K, Crean AM, Wintersperger BJ, et al. The relationship between cardiovascular magnetic resonance imaging measurement of extracellular volume fraction and clinical outcomes in adults with repaired tetralogy of Fallot. Eur Heart J Cardiovasc Imaging 2018;19:777–84.
[107] Kozak MF, Redington A, Yoo SJ, et al. Diffuse myocardial fibrosis following tetralogy of Fallot repair: a T1 mapping cardiac magnetic resonance study. Pediatr Radiol 2014;44:403–9.
[108] Kellman P, Wilson JR, Xue H, et al. Extracellular volume fraction mapping in the myocardium, part 2: initial clinical experience. J Cardiovasc Magn Reson 2012;14:64.
[109] Liu CY, Liu YC, Wu C, et al. Evaluation of age-related interstitial myocardial fibrosis with cardiac magnetic resonance contrast-enhanced T1mapping: MESA (Multi-Ethnic Study of Atherosclerosis). J Am Coll Cardiol 2013;62:1280–7.
[110] Piechnik SK, Ferreira VM, Lewandowski AJ, et al. Normal variation of magnetic resonance T1 relaxation times in the human population at 1.5 T using ShMOLLI. J Cardiovasc Magn Reson 2013;15:13.
[111] Chow K, Flewitt JA, Green JD, et al. Saturation recovery single-shot acquisition (SASHA) for myocardial T 1 mapping. Magn Reson Med 2014;71:2082–95.
[112] Reiter U, Reiter G, Dorr K, et al. Normal diastolic and systolic myocardial T1 values at 1.5-T MR imaging: correlations and blood normalization. Radiology 2014;271:365–72.
[113] Dabir D, Child N, Kalra A, et al. Reference values for healthy human myocardium using a T1 mapping methodology: results from the International T1 Multicenter cardiovascular magnetic resonance study. J Cardiovasc Magn Reson 2014;16:69.
[114] Giri S, Shah S, Xue H, et al. Myocardial T2 mapping with respiratory navigator and automatic nonrigid motion correction. Magn Reson Med 2012;68:1570–8.
[115] Westwood M, Anderson LJ, Firmin DN, et al. A single breath-hold multiecho T2* cardiovascular magnetic resonance technique for diagnosis of myocardial iron overload. J Magn Reson Imaging 2003;18:33–9.
[116] Pepe A, Positano V, Santarelli MF, et al. Multislice multiecho T2* cardiovascular magnetic resonance for detection of the heterogeneous distribution of myocardial iron overload. J Magn Reson Imaging 2006;23:662–8.
[117] Kirk P, Smith GC, Roughton M, et al. Myocardial T2* is not affected by ageing, myocardial fibrosis, or impaired left ventricular function. J Magn Reson Imaging 2010;32:1095–8.